# Coarsening Kinetics of a Two Phase Mixture with Highly Disparate Diffusion Mobility

G. Sheng[1,*], T. Wang[2], Q. Du[3,1], K. G. Wang[4], Z. K. Liu[1] and L. Q. Chen[1]

[1] *Department of Materials Science and Engineering, Pennsylvania State University, University Park, PA 16802, USA.*

[2] *Department of Materials Science and Engineering, Iowa State University, Ames, IA 50011, USA.*

[3] *Department of Mathematics, Pennsylvania State University, University Park, PA 16802, USA.*

[4] *Physics and Space Science Department, Materials Science & Nanotechnology Institute, Florida Institute of Technology, Melbourne, FL 32901, USA.*

**Abstract.** The coarsening kinetics of a two-phase mixture with a large diffusional mobility disparity between the two phases is studied using a variable-mobility Cahn-Hilliard equation. The semi-implicit spectral numerical technique was employed, and a number of interpolation functions are considered for describing the change in diffusion mobility across the interface boundary from one phase to another. The coarsening rate of domain size was measured using both structure and pair correlation functions as well as the direct computation of particle sizes in real space for the case that the coarsening phase consists of dispersed particles. We discovered that the average size $(\overline{R})$ versus time $(t)$ follows the $\overline{R}^{10/3} \propto t$ law, in contrast to the conventional LSW theory, $\overline{R}^3 \propto t$, and the interface-diffusion dominated two-phase coarsening, $\overline{R}^4 \propto t$.

## 1 Introduction

Coarsening is a kinetic process driven by the reduction in the total interfacial energy of a microstructure. As the mechanical properties of a material are critically determined

*Corresponding author. *Email addresses:* shengguang@psu.edu (G. Sheng), taowang@iastate.edu (T. Wang), qdu@math.psu.edu (Q. Du), kwang@fit.edu (K. G. Wang), Dr.Liu@psu.edu (Z. K. Liu), lqc3@psu.edu (L. Q. Chen)

by the degree of microstructure coarsening, it has been a subject of interest in materials science and engineering for over the last half century [1–4].

The first formal theory of coarsening was developed more than 40 years ago by Lifshitz and Slyozov [5], and Wagner [6], i.e. the so-called LSW theory which predicts that the cube of average particle size, $\overline{R}$, is linearly proportional to time $t$, i.e.,

$$\overline{R}^3 - \overline{R}_0^3 = kt,$$

where $k$ is the rate constant and $\overline{R}_0$ is the average length at time $t = 0$, and the particle sizes normalized by the average size have a unique distribution which is independent of time. LSW theory assumes that precipitates are spherical and the volume fraction of the coarsening phase is zero. Many attempts to improve the LSW theory by relaxing the zero volume fraction assumption [Ardell [7], Tsumuraya and Miyata [8], Asimow [9], Sarian and Weart [10], Aubauer [11, 12], Brailsford and Wynblatt [13], Voorhees and Glicksman [14], Marqusee and Ross [15], Tokuyama and Kawasaki [16], Marsh and Glicksman [17], and Davies et al. [18]] do not fundamentally change the cubic coarsening kinetics. The LSW cubic law for bulk-diffusion-dominated coarsening was confirmed by numerical simulations using a constant-mobility Cahn-Hilliard equation [19–22] which takes into the effect of non-spherical particle morphologies as well as volume fractions.

There have also been a number of studies using the Cahn-Hilliard equation with the scaled variable mobility term

$$M = 1 - aC^2,$$

where $C = C(\mathbf{r}, t)$ is the compositional field, [Langer et al. [23], Kitahara et al. [24], Lacasta et al. [25] and Zhu et al. [26]] which allow one to model two common diffusion mechanisms: a constant mobility describing bulk-diffusion-dominated coarsening ($\overline{R} \propto t^{1/3}$) for $a = 0$ and the coarsening dominated by interfacial diffusion for $a = 1$. These works convincingly showed that the coarsening of a two-phase microstructure with predominantly interfacial diffusion leads to $\overline{R}^4 \propto t$ [27] power law while for all other values of a between 0 and 1 ($a \neq 1$), there is a cross-over between $\overline{R} \propto t^{1/3}$ and $\overline{R} \propto t^{1/4}$. Based on dimensionality argument, Bray et al. [28] derived a growth law

$$\overline{R}^{(3+\alpha)} \propto t$$

corresponding to the Cahn-Hilliard equation with a composition-dependent-mobility,

$$M \propto (1 - C^2)^\alpha,$$

in the Lifshitz-Slyozov limit where the minority phase occupies a vanishingly small volume fraction. This theory successfully predicted two classic coarsening kinetics regimes: $\alpha = 0$ for diffusion-limited coarsening and $\alpha = 1$ for interfacial diffusion dominated coarsening.

However, there is a class of two-phase systems in which the diffusional mobility in the coarsening phase is dramatically smaller than the matrix or the other phase in a two-phase mixture, common in many engineering alloys. For example, the diffusion coefficient of Al in L1$_2$ is at least an order of magnitude smaller than that in the Ni-matrix in Ni-base alloys. It has recently been suggested that such dramatic differences in diffusivities may result in fundamentally different coarsening kinetics. Based on the experimental investigation in Ni-based alloys, Ardell and Ozolins argued that the coarsening of coherent particles in which the solute diffusivity is much lower than that in the matrix is controlled by diffusion through the precipitate-matrix interface, leading to $\overline{R}^2 \propto t$ kinetics [29]. In contrast, in another experimental study, Seidman et al. [30] investigated the kinetics of $\gamma'$ coarsening in Ni-5.2 at.%Al-14.2 at.%Cr at 873K by 3D Atom Probe Tomography (APT) and reported a value of 3.33±0.45 for $n$ in $\overline{R}^n \propto t$. In this case the mobility of Al in the precipitate is about one order of magnitude smaller than that in the matrix [31], according to the atomic mobility database of the Ni-Al-Mo system [32] as a reference, which is similar to Ni-Al-Cr system.

The main objective of this work is, therefore, to systematically study the coarsening kinetics with large diffusional mobility disparity between the coarsening phase and the matrix. We employ a variable-mobility Cahn-Hilliard equation [33] which allows us to vary the diffusion coefficients by orders of magnitude within a two-phase mixture. Long-time simulations under various mobility functions were made possible using the semi-implicit numerical technique [26, 34]. We study the coarsening kinetics of both interconnected two-phase microstructures and isolated precipitate particles embedded in a matrix. The kinetics is analyzed by determining the average spatial scale of a two-phase mixture as a function of time for different ratios of diffusivity in the precipitates and in the matrix.

## 2   Variable mobility Cahn-Hilliard equation

We employ a single compositional field $C(\mathbf{r},t)$ to describe two-phase microstructure. Within the bulk of the two phases, the composition field is equal or close to their equilibrium values determined by thermodynamics. The composition is continuous across the interfaces from one phase to another. The total free energy of an inhomogeneous two-phase mixture is then described by the Cahn-Hilliard free energy functional [33],

$$F = \int_V \left[ f(C) + \frac{1}{2}\kappa(\nabla C)^2 \right] dV, \tag{2.1}$$

where $f(C)$ is the local free-energy density and $\kappa$ is the gradient energy coefficient that can be related to inter-atomic interaction parameters.

The evolution of the composition profile is then modeled by the Cahn-Hilliard equation [33],

$$\frac{\partial C}{\partial t} = \nabla \left( M \nabla \frac{\delta F}{\delta C} \right), \tag{2.2}$$

where $t$ is time, $M$ is the diffusional mobility, and $\delta F/\delta C$ is the variational derivative of the total free energy.

The difference in diffusion coefficients between the two phases is described by a composition-dependent mobility $M(C)$. With a double-well potential function for the local free-energy density,

$$f(C) = -\frac{1}{2}C^2 + \frac{1}{4}C^4,$$

the Cahn-Hilliard equation with composition-dependent mobility can be presented in a scaled form as

$$\frac{\partial C(\mathbf{r},t)}{\partial t} = \nabla \cdot \left( M(C)\nabla[-C+C^3-\kappa\nabla^2 C] \right), \tag{2.3}$$

which is similar to the form presented by Langer et al. [23] and Kitahara and Imada [24].

# 3   Semi-implicit Fourier spectral method

A high-quality numerical study of the Cahn-Hilliard equation firstly requires a large system size to have good statistics and to minimize the effect of periodicity imposed by periodic boundary conditions. Secondly, longer enough evolution time is necessary in order to understand the scaling behavior of morphological patterns. Our previous studies [26, 34] showed the semi-implicit Fourier-spectral method of the variable mobility Cahn-Hilliard equation made it possible to use large time steps without losing stability and accuracy. Consequently, we can perform long-time simulations with large system sizes.

We use a Fourier spectral approximation to (2.3) by transforming the partial differential equation into a sequence of ordinary differential equations in the Fourier space,

$$\frac{\partial \tilde{C}(\mathbf{k},t)}{\partial t} = i\mathbf{k} \cdot \left\{ M(C)[i\mathbf{k}'(\{-C+C^3\}'_{\mathbf{k}} + \kappa k'^2 \tilde{C}(\mathbf{k}',t))]_{\mathbf{r}} \right\}_{\mathbf{k}}', \tag{3.1}$$

where $\mathbf{k} = (k_1, k_2)$ is a vector in the Fourier space,

$$k = \sqrt{k_1^2 + k_2^2}$$

is the magnitude of $\mathbf{k}$, and $C(\tilde{\mathbf{k}},t)$ and $\{-C+C^3\}'_{\mathbf{k}}$ represent the Fourier transform of $C(\mathbf{r},t)$ and the bulk driving force term $-C+C^3$, respectively.

For a constant mobility Cahn-Hilliard equation with $M(C) = 1$, Eq. (3.1) will be reduced to

$$\frac{\partial \tilde{C}(\mathbf{k},t)}{\partial t} = -k^2\{-C+C^3\}_{\mathbf{k}} - \kappa k^4 \tilde{C}(\mathbf{k},t). \tag{3.2}$$

Different from the traditional explicit Euler Fourier spectral method, here we treat the linear fourth-order operators implicitly and the nonlinear terms explicitly. Then the resulting first-order semi-implicit Fourier-spectral scheme under a constant mobility could

be represented as [26, 34]:

$$(1+\Delta t\kappa k^4)\tilde{C}^{n+1}(\mathbf{k},t)=\tilde{C}^n(\mathbf{k},t)-\Delta tk^2\{\tilde{g}(C^n(\mathbf{k},t))\}_{\mathbf{k}}, \tag{3.3}$$

where $g(C)=-C+C^3$. For a variable mobility Cahn-Hilliard equation, the explicit Euler Fourier spectral treatment of (3.1) is

$$\frac{\tilde{C}^{n+1}(\mathbf{k},t)-\tilde{C}^n(\mathbf{k},t)}{\Delta t}=i\mathbf{k}\cdot\left\{M(C)[i\mathbf{k}'(\{-C+C^3\}^n_{\mathbf{k}'}+\kappa k'^2\tilde{C}^n(\mathbf{k}',t))]_{\mathbf{r}}\right\}_{\mathbf{k}}. \tag{3.4}$$

The idea of semi-implicit treatment for the above equation is to split the variable mobility $M(C)$ into $A$ and $M(C)-A$, where $A$ is a suitable constant, and the scheme could be written as [34]:

$$\left(1+A\Delta t\kappa k^4\right)\tilde{C}^{n+1}(\mathbf{k},t)$$
$$=\left(1+A\Delta t\kappa k^4\right)\tilde{C}^n(\mathbf{k},t)+\Delta ti\mathbf{k}\cdot\left\{M(C)\times\left[i\mathbf{k}'(\{-C+C^3\}^n_{\mathbf{k}'}+\kappa k'^2\tilde{C}^n(\mathbf{k}',t))\right]_{\mathbf{r}}\right\}_{\mathbf{k}'}, \tag{3.5}$$

where $A=\frac{1}{2}[\max(M(C))+\min(M(C))]$. In this paper, all the composition dependent mobility functions $M(C)$ has the scaled maximum value $M=1$ and minimum $M=0$, thus $A=1/2$ is a good approximation for all the simulations.

## 4  Simulation results

To model the coarsening kinetics, the simple double-well free energy function

$$f(C)=-\frac{1}{2}C^2+\frac{1}{4}C^4$$

has two minima located at $C_p=-1$ and $C_m=+1$, respectively, representing the equilibrium compositions of the two phases.

To introduce the diffusional mobility difference between the two phases in a two-phase mixture, we employ a number of functions to describe its compositional dependence (Table 1). For example, for the case of $M=(1+C)/2$, the diffusional mobility in the $C_p=-1$ phase is reduced to zero, whereas that in the $C_m=+1$ phase is close to one. This produces a large mobility difference between the two phases.

The simulations are performed on a 2D square domain using $1024\times1024$ grid points with a grid size 1.0 and $2048\times2048$ grid points with a grid size 0.5. For both cases, the time step $\Delta t$ is taken to be 1.0. We consider two overall compositions values: $C_0=0$ for interconnected two-phase microstructure with 50% volume fraction for each phase and $C_0=0.4$ for coarsening of isolated precipitate particles ($\sim$30% volume fraction) in a continuous matrix. Periodic boundary conditions are employed. The system is initially prepared in a homogeneous state by assigning a random number to each grid point around their overall composition. The random numbers are uniformly distributed between 0.1 and $-0.1$ corresponding to a high-temperature initial state where the composition deviation from the average value is only caused by fluctuations. Averages are taken over 4 simulation runs using a different set of random numbers for each initial state.

Table 1: Scaled mobility function related to different mechanisms.

| Scaled Mobility function | $M_m(C=1)$ | $M_p(C=-1)$ | Mechanisms |
|---|---|---|---|
| 1 | 1 | 1 | bulk diffusion dominated |
| $1-C^2$ | $\approx 0$ | $\approx 0$ | interface controlled |
| $(1+C)/2$ | 1 | $\approx 0$ | huge mobility disparity |
| $\exp[0.5-1/(0.9+C)]$ | 1 | $\approx 0$ | huge mobility disparity |
| $0.45\sin(0.5\pi C)+0.55$ | 1 | 0.1 | 10 times difference |
| $0.495\sin(0.5\pi C)+0.505$ | 1 | 0.01 | 100 times difference |
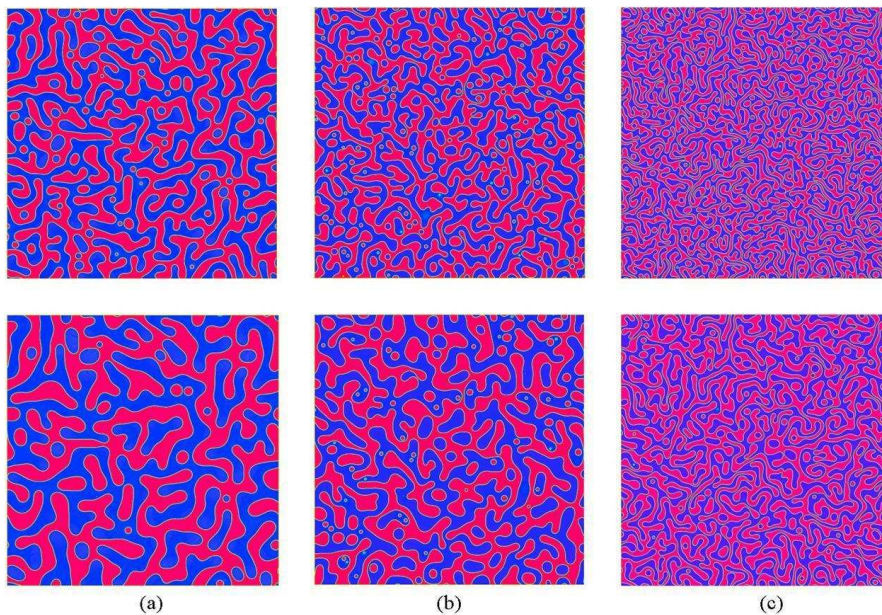


Figure 1: Morphological patterns during spinodal decomposition and subsequent coarsening for different dynamics at $t=10000$ (top) and $t=30000$ (bottom): (a) bulk-diffusion-dominated (b) large-mobility-disparity (c) interface-controlled.

## 4.1  Morphological evolution

Fig. 1 shows a typical example of temporal evolution of morphological patterns during coarsening using the mobility function $M=(1+C)/2$. For comparison, we also include a morphology obtained assuming $M=1$, i.e., bulk-diffusion-dominated coarsening, and $M=1-C^2$ for interface-diffusion-dominated dynamics, all started with the same initial condition. In Fig. 1, the local composition is represented by different colors with red representing positive values and blue negative values. For the critical overall composition at $C_0=0$, the volume fractions of the two phases are about the same, leading to interconnected morphologies. Domain coarsening is evident in all the three cases. However, the coarsening rates are quite different as shown from the morphology, and the
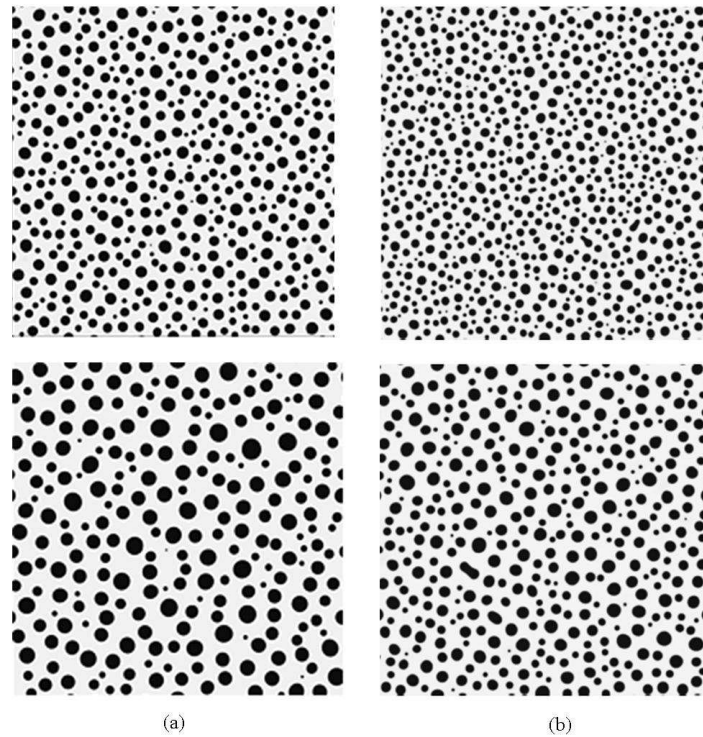
Figure 2: Morphological patterns during coarsening at 30% second-phase volume fraction from the numerical solutions of the Cahn-Hilliard Equation at $t = 10000$s (top) and $t = 30000$s (bottom) with (a) bulk-diffusion-dominated and (b) large disparity mobility.

average domain sizes decrease from left to right at both time steps, indicating that the bulk-diffusion-dominated case has the highest coarsening rate ($\overline{R} \propto t^{1/3}$) while interface-diffusion-dominated coarsening is the slowest ($\overline{R} \propto t^{1/4}$). The coarsening rate for the case of a large mobility disparity between the two phases is slower than the bulk-diffusion-dominated coarsening but faster than the interface-dominated case. Morphological patterns and coarsening rates obtained using other mobility functions from Table 1 show similar results as the $M = (1+C)/2$ case.

The microstructure evolution for a 30% volume fraction of the second phase ($C_0 = 0.4$) at two different times is shown in Fig. 2. Different from the previous case with almost equal volume fractions for the two phases, the two-phase microstructure in this case consists of second-phase particles dispersed in a continuous matrix phase. Due to the well-known Gibbs-Thomson effect, the chemical potential within the smaller particles is higher than that of the larger particles [25], and thus coarsening proceeds by a diffusional mass transfer process of atoms near the smaller particles towards the larger particles. The larger particles then grow at the expense of the smaller particles. According to the classical theory, it is expected that coarsening in this case is controlled by diffusion in the matrix. We compare the morphologies at a later time ($t = 30000$) for the constant mobility

and large-disparity-mobility cases. It can be seen that the total number of particles in Fig. 2(a) is less than that in Fig. 2(b) and hence the average particle size is larger for the constant mobility case, indicating that the coarsening rate is faster than the latter case. Since the diffusion coefficients in the matrix are the same for the case of a constant mobility $M=1$ and the case of a variable mobility $M=(1+C)/2$, the observed coarsening rate reduction for the latter case is mainly due to the reduction of the diffusion coefficient in the two-phase diffuse-interface regions, i.e., the reduction of interface diffusion.

## 4.2 Coarsening kinetics

To analyze the coarsening kinetics, we employed a number of different approaches to determine the average length scale, $\overline{R}$, as a function of time, $t$, including the temporal structure function, pair correlation function as well as the direct counting of particle sizes in real space [21, 26, 35]. The time-dependent structure factor, $S(\mathbf{k},t)$, is defined as [21]

$$S(\mathbf{k},t)=\frac{1}{N}\left\langle \sum_{\mathbf{r}}\sum_{\mathbf{r}'}e^{-i\mathbf{k}\cdot\mathbf{r}}[C(\mathbf{r}+\mathbf{r}',t)C(\mathbf{r}',t)-\langle C(\mathbf{r},t)\rangle^2]\right\rangle, \qquad (4.1)$$

where both sums run over the lattice of linear size $L$ and $N=L^2$ is the total number of points in a two-dimensional lattice. For an isotropic microstructure, one can also define a circularly averaged structure factor $S(k,t)$.

The corresponding pair correlation function, $G(\mathbf{r},t)$, can be obtained from the structure function,

$$G(\mathbf{r},t)=\sum_{\mathbf{k}}e^{i\mathbf{k}\cdot\mathbf{r}}S(\mathbf{k},t). \qquad (4.2)$$

The circularly averaged and normalized correlation function, $g(r,t)$, is

$$g(r,t)=\frac{G(r,t)}{G(0,t)}, \qquad (4.3)$$

where $G(r,t)$ is the circularly averaged pair correlation function and

$$G(0,t)=\langle C^2(r)-\langle C(r)\rangle^2\rangle. \qquad (4.4)$$

The structure factor normalized by $G(0,t)$ is then

$$s(k,t)=S(k,t)/G(0,t). \qquad (4.5)$$

Fig. 3 shows an example of the normalized and circularly averaged structure function $s(k,t)$ at eight different time steps for the large-mobility-disparity dynamics at $C_0=0.0$. The lines are spline fits to the simulation data. As expected, as time increases, the maximum value of the structure function increases and shifts to lower $k$, indicating an increase in the real-space average length scale.
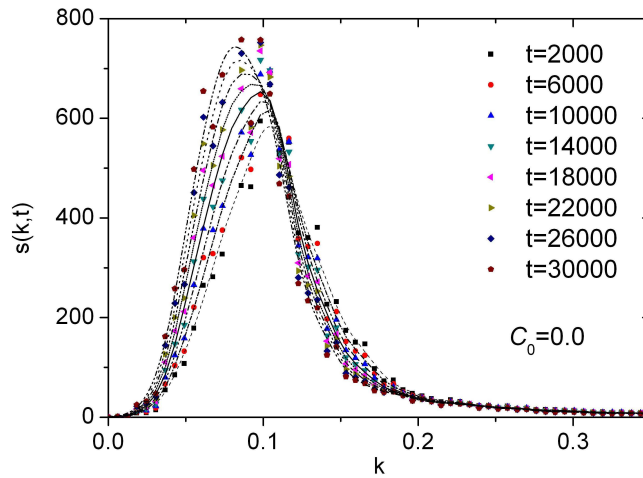
Figure 3: Structure factor $s(k,t)$ with wave vector $k$ at eight different time steps for large-mobility-disparity coarsening $(M=(1+C)/2, C_0=0.0)$.
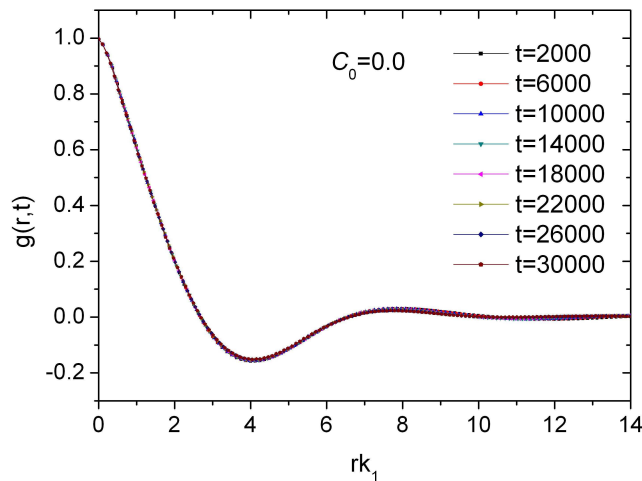


Figure 4: Normalized pair correlation function $g(r,t)$ with $rk_1$ for large-mobility-disparity coarsening $(M=(1+C)/2, C_0=0.0)$.

We also plotted the circularly averaged pair correlation function for the large mobility disparity dynamics at $C_0=0.0$ after $t=30000$. A main feature of the dynamical scaling is that the pair correlation function and the structure function $s(k,t)$ depend on time through the typical length scale $R(t)$ only. As is shown in Fig. 4, the pair correlation function exhibits characteristic oscillations about zero, which reflects the composition domain structure. Comparing with the earlier work on bulk-diffusion-dominated and interface-diffusion-dominated dynamics [21], the shape of the curve is rather similar in spite of their different dynamics.

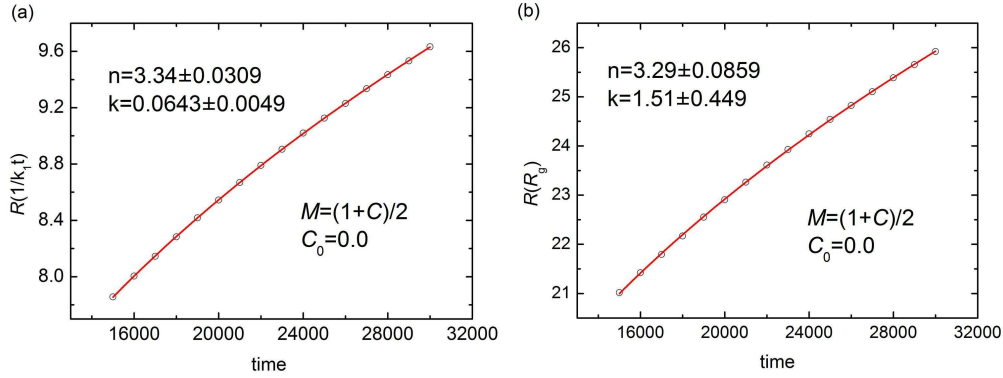The average domain size $R(t)$ can be obtained from the structure function [26,36], or

Figure 5: Nonlinear-fitting of the average domain size measured from different methods: $C_0 = 0.0$, grid size $1024 \times 1024$. (a) by $1/k_1(t)$, (b) by $R_g$.

the radial distribution function [25, 26] or direct counting of grid points in the real space. For example, one could characterize $R(t)$ using the first moment of $s(k,t)$, defined by

$$k_1(t) = \frac{\sum k s(k,t)}{\sum s(k,t)}. \tag{4.6}$$

One could also determine $R(t)$ by locating the first zero of the real-space pair correlation function, $R_g$, computed by a linear interpolation of the two points closest to the first sign change in $g(r,t)$.

Fig. 5 shows the time dependence of $R(t)$ characterized by both $1/k_1(t)$ (a) and $R_g$ (b) as a function of time for the case of average composition $C_0 = 0$ and mobility function $(1+C)/2$. To determine the coarsening exponent, we fit the data from the simulations to

$$\overline{R}^n - \overline{R}_0^n = kt, \tag{4.7}$$

where $\overline{R}(t)$ is the average domain size at a given time $t$, $\overline{R}_0$ is the initial length scale at $t=0$, and $k$ is the coarsening rate constant. The scatter circles are plots of the simulated data and solid lines are from non-linear fitting. Using non-linear regression, we found the exponent $n$ is around 3.3 for both $1/k_1(t)$ (a) and $R_g$ (b).

For the non-critical composition with particle coarsening case as shown in Fig. 2, we can also calculate the average size of spherical particles through direct measurement of individual particle sizes. As shown in Fig. 6(c), the average particle size is determined from a system with about 30% volume fraction. The diffusional mobility in precipitates is assumed to be near zero through the function $M = (1+C)/2$. Consistent with those determined from $1/k_1(t)$ (a) and $R_g$ (b), the corresponding coarsening exponent $n$ directly from counting the particle sizes is around 3.3.

Our simulation results demonstrate that, this $\overline{R}^{3.3} \propto t$ growth law is independent of the volume fraction of the second phase. In both Fig. 5 and Fig. 6, the growth laws for two initial average compositions, $C_0 = 0.0$ and $C_0 = 0.4$, have similar coarsening exponents which are very close to 3.3.
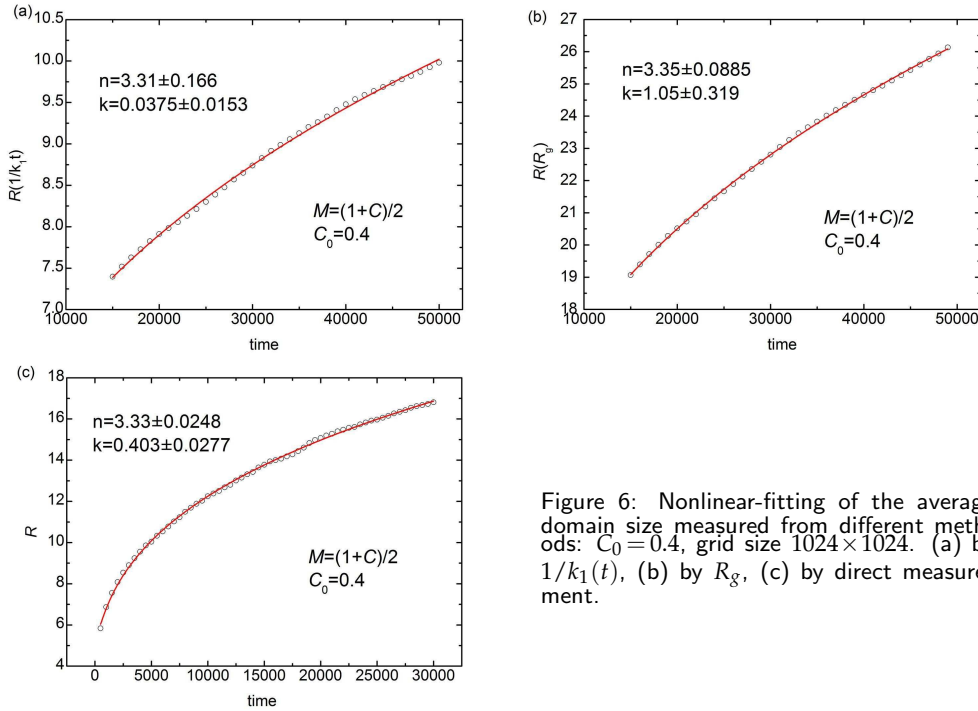
Figure 6: Nonlinear-fitting of the average domain size measured from different methods: $C_0 = 0.4$, grid size $1024 \times 1024$. (a) by $1/k_1(t)$, (b) by $R_g$, (c) by direct measurement.

## 5  Discussions

The coarsening time exponent, 3.3 or $\sim 10.0/3$, as presented in the result section above, was obtained using a specific mobility function

$$M = \frac{1}{2}(1+C). \tag{5.1}$$

The equilibrium compositions of the two phases are at $C = -1$ and $+1$ respectively. Therefore, this mobility function was expected to lead to a zero mobility in the phase with $C = -1$ and a finite mobility within the other phase with $C = +1$. However, it should be noted that due to the capillarity effect, the concentrations within the composition domains may not be exactly $+1$ or $-1$. Therefore, the mobility is not close to zero or one even with the mobility function $(1+C)/2$ (with $C = -1$ in the particles). To evaluate whether this capillarity effect has any significant effect on the coarsening kinetics, we conducted an additional test with the mobility function

$$M = \exp[0.5 - 1/(0.9 + C)], \tag{5.2}$$

which will result in a mobility which varies from 1.0 in the matrix to close to 0.0 very quickly across the interface. As shown in Fig. 7, this mobility function leads to a similar coarsening time exponent.
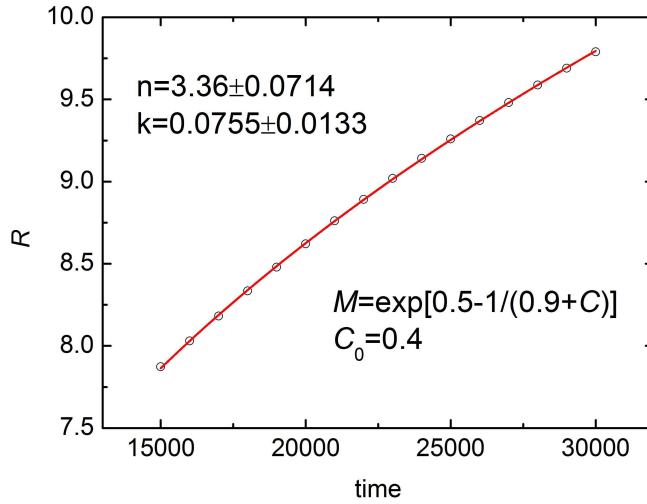
Figure 7: Nonlinear-fitting of the average domain size vs time using mobility function $M=\exp[0.5-1/(0.9+C)]$: $C_0=0.4$, grid size $1024\times1024$.
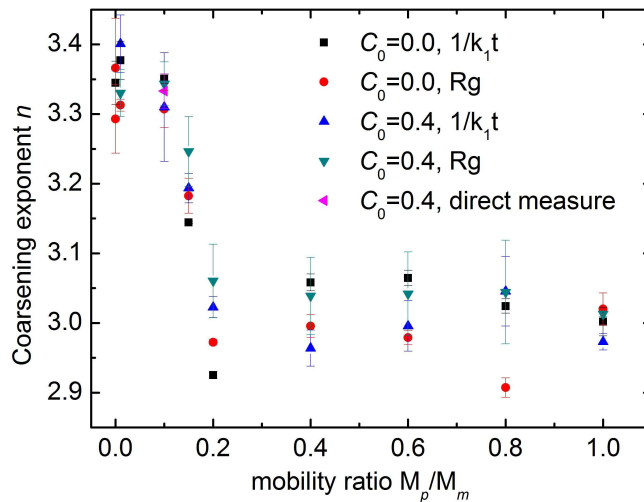


Figure 8: Coarsening exponents as a function of the different ratio between the mobility in precipitate $M_p$ and in matrix $M_m$ from different mobility functions. Scaling methods include $1/k_1(t)$, $R_g$ and direct measurement of the particle size (noncritical case), the data point at $M_p/M_m=0$ is taken from the function $M=(1+C)/2$ and $M=\exp[0.5-1/(0.9+C)]$.

To investigate how the degree of mobility disparity between the matrix and precipitate affect the coarsening kinetics, we also perform a series of simulations with different ratios between the mobility in precipitate $M_p$ and in matrix $M_m$ from $M_p/M_m=1$ to $M_p/M_m=0$ and measure the coarsening exponents. Fig. 8 represents the results as a function of mobility ratios from different mobility functions (Table 1). The error bars indicate the variation of data from non-linear fitting. The data at $M_p/M_m=0$ is collected from
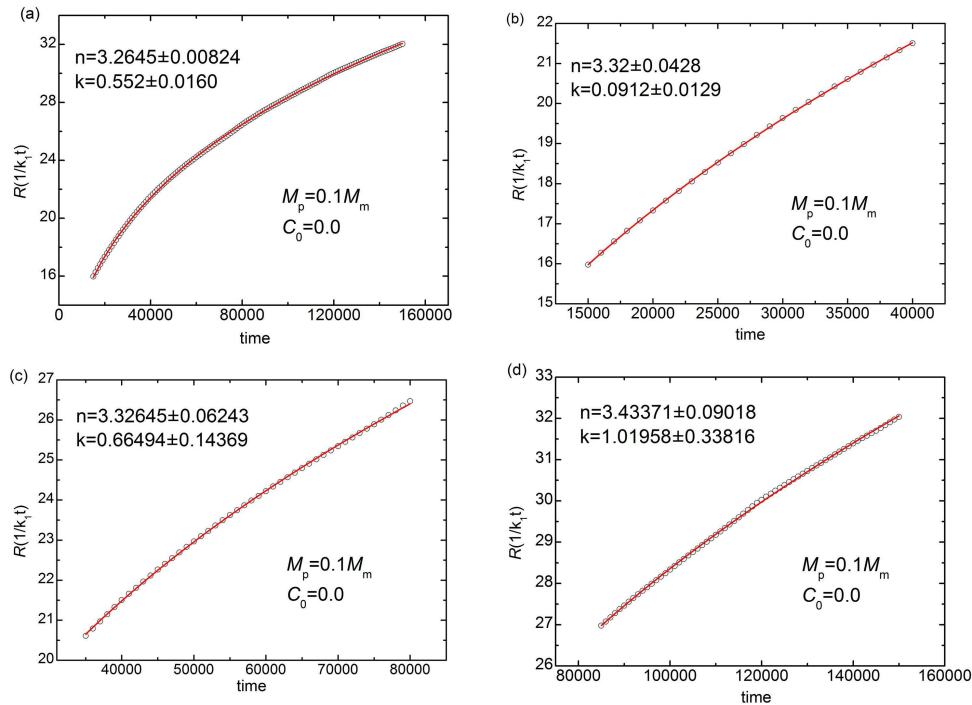
Figure 9: Nonlinear-fitting of the average domain size vs time at different time stages of coarsening at 10 times difference mobility: $C_0 = 0.0$, grid size $2048 \times 2048$. (a) overall, (b) beginning, (c) middle, (d) end.

the function (5.1) (Fig. 5 and Fig. 6) and (5.2) (Fig. 7), others are all from sine functions. Different symbols stand for the variation of measurement methods including $1/k_1(t)$, $R_g$ and direct measurement of the non-critical particle case (Fig. 6(c)). The coarsening mechanisms changes with mobility ratio could be divided into two groups. The coarsening exponent remains around 3.0, indicating a bulk diffusion controlled cubic law for mobility ratios $M_p/M_m$ from 1.0 to 0.8, 0.6, 0.4 until 0.2. The exponent increase from 3.0 ($M_p/M_m = 0.2$) to $3.3 \sim 3.4$ when the ratio continues reducing to around 0.1 and further, which indicates that an order of magnitude difference between the mobility in matrix and precipitate leads to the $\overline{R}^{3.3}$ law. The coarsening exponent stays with $3.3 \sim 3.4$ even with the mobility ratio reduced to near zero.

We also examined whether the coarsening time exponents at different stages might be different by running much longer simulations. Fig. 9 and Fig. 10 show the non-linear fitting results at different time stages during the coarsening process at different compositions and mobility ratios. The coarsening exponent $n$ remains within a close range around 3.3, demonstrating that the coarsening behavior is independent of the different time stages.

The predicted coarsening exponent from this work, 3.3 or $\sim 10/3$, seems to be consistent with experimental results on the coarsening kinetics of $\gamma'$ precipitates in Ni-5.2Al-
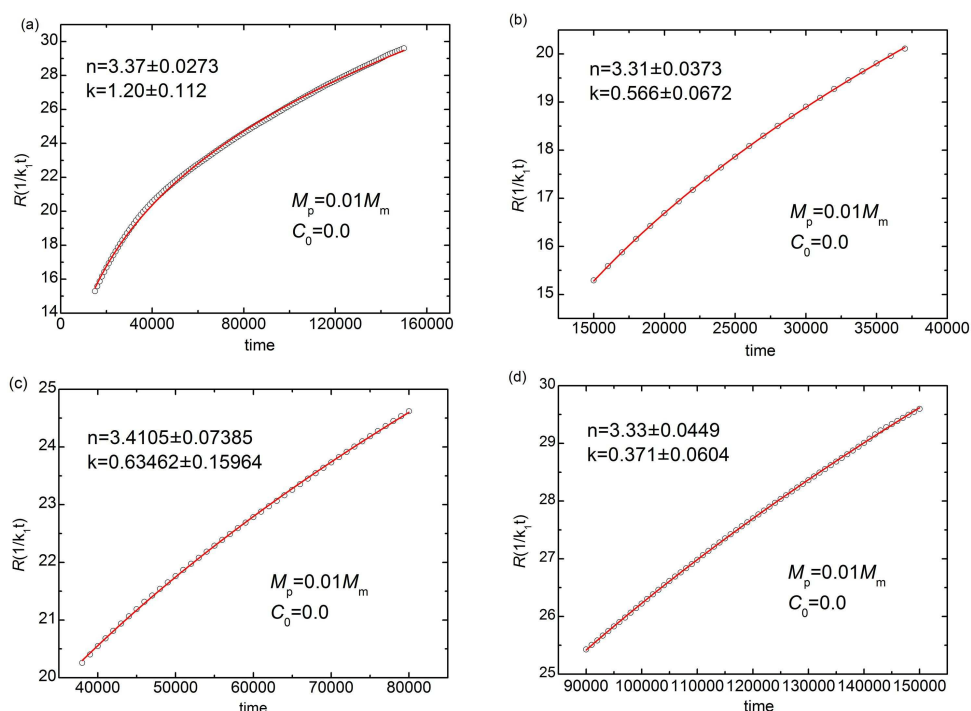
Figure 10: Nonlinear-fitting of the average domain size vs time at different time stages of coarsening at 100 times difference mobility: $C_0 = 0.0$, grid size $2048 \times 2048$. (a) overall, (b) beginning, (c) middle, (d) end.

14.2Cr aged at 873 K [30]. The diffusional mobility in the precipitates is about one order of magnitude smaller than that in the matrix. The average radius $\overline{R}$ of the $\gamma'$ precipitates is determined by Atom Probe Tomographic and a coarsening exponent of $3.33 \pm 0.45$ is obtained.

## 6  Summary

The coarsening kinetics with large diffusional mobility disparity was studied using the variable mobility Cahn-Hilliard equation. It is shown that the morphological pattern evolution in large-mobility-disparity coarsening is slower than the diffusion-limited but faster than interface-controlled coarsening, closely related to the slow interface diffusion. Based on our simulation results, we obtained a growth law

$$\overline{R}^{3.3} \propto t$$

for two-phase systems with mobility disparity differing by one order of magnitude or higher, which is shown to be also independent of second-phase volume fraction in the volume fraction range studied.

## Acknowledgments

## References

[1] K.G. Wang and M.E. Glicksman, Ostwald Ripening in Materials Processing. In: Materials Processing Handbook, edited by J. Groza, J. Shackelford, E. Lavernia and M. Powers, CRC Press, 2007.

[2] A.J. Bray, Theory of phase-ordering kinetics, Adv. Phys., 51 (2002), pp. 481-587.

[3] A.J. Bray, Theory of phase-ordering kinetics, Adv. Phys., 43 (1994), pp. 357-459.

[4] A. Baldan, Progress in Ostwald ripening theories and their applications to nickel-base superalloys - Part I: Ostwald ripening theories, J. Mater. Sci., 37 (2002), pp. 2171-2202.

[5] I.M. Lifshitz, V.V. Slyozov, The kinetics of precipitation from supersaturated solid solutions, J. Phys. Chem. Sol.,19 (1961), pp. 35-50.

[6] C. Wagner, Theorie der Alterung vonNiederschlagen dursch Umlosen, Z. Electrochem., 65 (1961), pp. 581-594.

[7] A.J. Ardell, The effect of volume fraction on particle coarsening: theoretical considerations, Acta Metall., 20 (1972), pp. 61-71.

[8] K. Tsumuraya, Y. Miyata, Coarsening models incorporating both diffusion geometry and volume fraction of particles, Acta Metall., 31 (1983), pp. 437-452.

[9] R. Asimow, Clustering kinetics in binary alloys, Acta Metall., (11) 1963, pp. 72-73.

[10] S. Sarian, H.W Weart, Kinetics of coarsening of spherical particles in a liquid matrix, J. Appl. Phys., 37 (1966), pp. 1675-1681.

[11] H.P. Aubauer, Two-phase systems with dispersed particles of a stable size-I. Theory, Acta Metall., 20 (1972), pp. 165-172.

[12] H.P. Aubauer, Two-phase systems with dispersed particles of a stable size-II. Numerical evaluation, Acta Metall., 20 (1972), pp. 173-180.

[13] A.D. Brailsford, P. Wynblatt, The dependence of ostwald ripening kinetics on particle volume fraction, Acta Metall., 27(1979), pp. 489-497.

[14] P.W. Voorhees and M.E. Glicksman, Ostwald ripening during liquid phase sintering-Effect of volume fraction on coarsening kinetics, Met. Trans., 15A (1984), pp. 1081-1088.

[15] J.A. Marqusee and J. Ross, Theory of Ostwald ripening: competitive growth and its dependence on volume fraction, J. Chem. Phys., 80 (1984), pp. 536-543.

[16] M. Tokuyama, K. Kawasaki, Statistic-mechanical theory of coarsening of spherical droplets, Physica A., 123 (1984), pp. 386-411.

[17] S.P. Marsh, M.E. Glicksman, Kinetics of phase coarsening in dense systems, Acta Mater., 44 (1996), pp. 3761-3771.

[18] C.K.L Davies, P. Nash, R.N. Stevens, Effect of volume fraction of precipitation on Ostwald ripening, Acta Metall., 28 (1980), pp. 179-189.

[19] T.M. Rogers, K.R. Elder and R.C. Desai., Numerical study of the late stages of spinodal decomposition, Phys. Rev. B, 37 (1988), pp. 9638-9649.

[20] T.M. Rogers and R.C. Desai, Numerical study of late-stage coarsening for off-critical quenches in the Cahn-Hilliard equation of phase separation, Phys. Rev. B, 39 (1989), pp. 11956-11964.

[21] A. Chakrabarti, R. Toral, and J.D. Gunton, Late-stage coarsening for off-critical quenches: Scaling functions and the growth law, Phys. Rev. E, 47 (1993), pp. 3025-3038.

[22] T. Kupper and N. Masbaum, Simulation of particle growth and Ostwald ripening via the Cahn-Hilliard equation, Acta. Metall. Mater., 42 (1994), pp. 1847-1858.

[23] J.S. Langer, M. Bar-on and H.D. Miller, New computational method in the theory of spinodal decomposition, Phys. Rev. A, 11(1975), pp. 1417-1429.

[24] K. Kitahara and M. Imada, On the Kinetic Equations for Binary Mixtures, Prog. Theor. Phys. Suppl., 64 (1978), pp. 65-73.

[25] A.M. Lacasta, A. Hernandez-Machado, J.M. Sancho, and R. Toral, Domain growth in binary mixtures at low temperatures, Phys. Rev. B, 45 (1992), pp. 5276-5281.

[26] J.Z. Zhu, L.Q. Chen, J. Shen and V. Tikare, Coarsening kinetics from a variable-mobility Cahn-Hilliard equation: application of a semi-implicit Fourier spectral method, Phys. Rev. E, 60 (1999), pp. 3564-3572.

[27] H. Furukawa, A dynamic scaling assumption for phase-separation, Adv. Phys., 34 (1985), pp. 703-750.

[28] A.J. Bray and C.L. Emmott, Lifshitz-Slyozov scaling for late-stage coarsening with an order-parameter-dependent mobility, Phys. Rev. B, 52 (1995), pp. R685-R688.

[29] A.J. Ardell, V. Ozolins, Trans-interface diffusion-controlled coarsening, Nat. Mater. 4 (2005), pp. 309-316.

[30] D. Seidman, C. Sudbrack, K. Yoon, The use of 3-D atom-probe tomography to study nickel-based superalloys, JOM, 58 (2006), pp. 34-39.

[31] T. Wang, G. Sheng, Z.K. Liu and L.Q. Chen, Coarsening kinetics of gamma ′ precipitates in the Ni-Al-Mo system, Acta Mater., 56 (2008), pp. 5544-5551.

[32] T. Wang, Ph.D. Thesis. University Park, PA: The Pennsylvania State University;2006.

[33] J.W. Cahn and J.E. Hilliard, Free energy of a nonuniform system. I. Interfacial free energy, J. Chem. Phys., 28 (1958), pp. 258-267.

[34] L.Q. Chen and J. Shen, Applications of semi-implicit Fourier-spectral method to phase field equations, Comput. Phys. Commun., 108 (1998), pp. 147-158.

[35] D. Raabe, Computational Materials Science: The simulations of materials microstructures and properties. Wiley-VCH, New York, 1998.

[36] P. Fratzl, J.L. Lebowitz, O. Penrose, J. Amar, Scaling functions, self-similarity, and the morphology of phase separating systems, Phys. Rev. B, 44 (1991), pp. 4794-4811.